BIOCHEMISTRY
including biophysical chemistry & molecular biology
Article

Biochemistry **2011,** *50,* 1483–1491 1483
DOI: 10.1021/bi101871f

Biochemical and Structural Characterization of WlbA from *Bordetella pertussis* and *Chromobacterium violaceum*: Enzymes Required for the Biosynthesis of 2,3-Diacetamido-2,3-dideoxy-D-mannuronic Acid[†,‡]

James B. Thoden and Hazel M. Holden*

Department of Biochemistry, University of Wisconsin, Madison, Wisconsin 53706, United States

Received November 23, 2010; Revised Manuscript Received January 12, 2011

ABSTRACT: The unusual sugar 2,3-diacetamido-2,3-dideoxy-D-mannuronic acid, or ManNAc3NAcA, has been observed in the lipopolysaccharides of both pathogenic and nonpathogenic Gram-negative bacteria. It is added to the lipopolysaccharides of these organisms by glycosyltransferases that use as substrates UDP-ManNAc3NAcA. Five enzymes are ultimately required for the biosynthesis of UDP-ManNAc3NAcA starting from UDP-*N*-acetylglucosamine. The second enzyme in the pathway, encoded by the *wlba* gene and referred to as WlbA, catalyzes the NAD-dependent oxidation of the C-3′ hydroxyl group of the UDP-linked sugar. Here we describe a combined structural and functional investigation of the WlbA enzymes from *Bordetella pertussis* and *Chromobacterium violaceum*. For this investigation, ternary structures were determined in the presence of NAD(H) and substrate to 2.13 and 1.5 Å resolution, respectively. Both of the enzymes display octameric quaternary structures with their active sites positioned far apart. The octamers can be envisioned as tetramers of dimers. Kinetic studies demonstrate that the reaction mechanisms for these enzymes are sequential and that they do not require α-ketoglutarate for activity. These results are in sharp contrast to those recently reported for the WlbA enzymes from *Pseudomonas aeruginosa* and *Thermus thermophilus*, which function via ping-pong mechanisms that involve α-ketoglutarate. Taken together, the results reported here demonstrate that there are two distinct families of WlbA enzymes, which differ with respect to amino acid sequences, quaternary structures, active site architectures, and kinetic mechanisms.

The incidence of whooping cough has risen steadily in the past few years with several states, including Ohio and California, witnessing their largest outbreaks in 25 and 60 years, respectively. Whereas the disease is often mild in adults, it can result in significant morbidity and mortality rates in children under the age of 2. The causative agent of whooping cough is *Bordetella pertussis*, a Gram-negative bacterium that infects humans by colonizing lung epithelial cells. As observed in most other Gram-negative bacteria, *B. pertussis* has a lipopolysaccharide or LPS, which serves as the major structural component for its outer membrane. The LPS is composed of lipid A, the core polysaccharide, and the *O*-antigen. A rather rare diacetylated sugar, 2,3-diacetamido-2,3-dideoxy-D-mannuronic acid or ManNAc3NAcA,[1] is found in the *O*-antigen of *B. pertussis*, and it has also been observed in the LPS of *Pseudomonas aeruginosa* serogroup O2 (*1*). The physiological importance of the *O*-antigen in *B. pertussis* is underscored by the fact that it confers resistance to complement-mediated cell lysis (*2*), and it also prevents clearance of the bacterium by the pulmonary surfactant protein A (*3*).

Five enzymes are required for the production of UDP-ManNAc3NAcA in both *B. pertussis* and *P. aeruginosa* as indicated in Scheme 1 (*4*−*6*). The focus of this investigation is on the enzyme WlbA, which catalyzes the second step in the pathway, namely, the oxidation of UDP-*N*-acetyl-D-glucosaminuronic acid (UDP-GlcNAcA) to UDP-2-acetamido-2-deoxy-3-oxo-D-glucuronic acid (UDP-3-keto-GlcNAcA). The enzyme is NAD-dependent, and a previous biochemical study of the protein from *P. aeruginosa* PAO1 demonstrated that it employs α-ketoglutarate to regenerate the oxidized cofactor necessary for the next round of catalysis (*6*). Indeed, α-ketoglutarate is absolutely required for catalysis by the *P. aeruginosa* enzyme (*6*). We recently reported the three-dimensional structures of WlbA from both *P. aeruginosa* and *Thermus thermophilus* in complex with NAD(H), with NAD(H) and α-ketoglutarate, and with NAD(H) and UDP-GlcNAcA. The enzymes from both bacterial species assumed unusual tetrameric quaternary structures with the NAD(H) moieties closely situated to one another as can be seen in Figure 1 (*7*). The individual subunits of the tetramers displayed overall folds similar to that reported for glucose−fructose

[†]This research was supported in part by an NIH grant (DK47814 to H.M.H.).

[‡]X-ray coordinates have been deposited in the Research Collaboratory for Structural Bioinformatics, Rutgers University, New Brunswick, NJ (accession numbers 3Q2I and 3Q2K).

*To whom correspondence should be addressed. E-mail: Hazel_Holden@biochem.wisc.edu. Fax: 608-262-1319. Phone: 608-262-4988.

[1]Abbreviations: HEPPS, 3-[4-(2-hydroxyethyl)-1-piperazinyl]propanesulfonic acid; HPLC, high-performance liquid chromatography; IPTG, isopropyl β-D-thiogalactopyranoside; LB, Luria−Bertani; NAD(H), nicotinamide adenine dinucleotide; NiNTA, nickel nitrilotriacetic acid; PCR, polymerase chain reaction; TEV, tobacco etch virus; Tris, 2-amino-2-(hydroxymethyl)propane-1,3-diol; UDP, uridine 5′-phosphate; UDP-GlcA, UDP-D-glucuronic acid; UDP-GlcNAc, UDP-*N*-acetyl-D-glucosamine; UDP-GlcNAcA, UDP-*N*-acetyl-D-glucosaminuronic acid; UDP-3-keto-GlcNAcA, UDP-2-acetamido-2-deoxy-3-oxo-D-glucuronic acid; UDP-GlcNAc3NA, UDP-2-acetamido-3-amino-2,3-dideoxy-D-glucuronic acid; UDP-GlcNAc3NAcA, UDP-2,3-diacetamido-2,3-dideoxy-D-glucuronic acid; UDP-ManNAc3NAcA, UDP-2,3-diacetamido-2,3-dideoxy-D-mannuronic acid.

Published on Web 01/17/2011

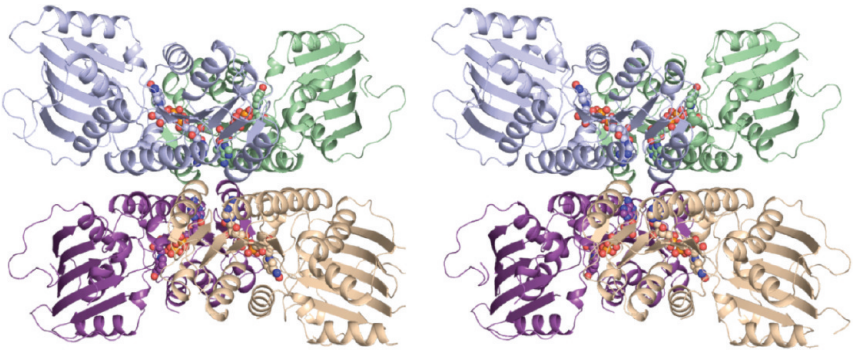

FIGURE 1: Structure of WlbA from *P. aeruginosa*. A stereoview of the WlbA tetramer is shown with the individual subunits colored in green, wheat, purple, and blue. The NAD(H) cofactors are displayed as space-filling representations. This figure and Figures 3−6 were prepared with PyMOL (*18*).

Scheme 1

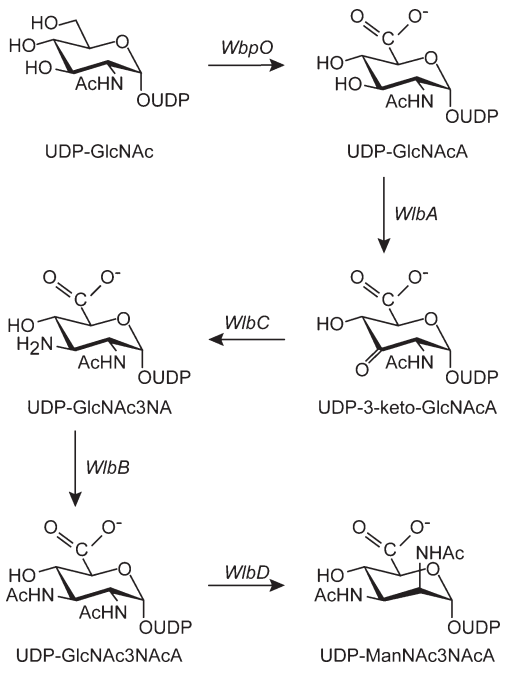

oxidoreductase from *Zymomonas mobilis* (*8*). Strikingly, the UDP-linked substrates adopted highly unusual curved conformations in the active site clefts of the tetramers. In addition to the structural studies, we showed that these two enzymes catalyzed their reactions via ping-pong mechanisms (*7*).

Given that the WlbA enzymes from *P. aeruginosa* and *B. pertussis* catalyze the same reactions in the biosynthesis of UDP-ManNAc3NAcA (*4*), we anticipated that the structure of the *B. pertussis* enzyme would adopt a similar molecular architecture to that shown in Figure 1. We also assumed that the *B. pertussis* WlbA would use α-ketoglutarate to regenerate the oxidized cofactor. To our surprise, all attempts to solve the structure of the *B. pertussis* enzyme in the presence of α-ketoglutarate failed. Likewise, we were never able to demonstrate the recycling mechanism with the *B. pertussis* enzyme *in vitro*.

Here we report the structure of the *B. pertussis* enzyme in complex with NAD(H) and its UDP-linked substrate. Additionally, we describe the structure of WlbA from *Chromobacterium violaceum*, a Gram-negative bacterium that produces the antibiotic violacein (*9*). The *B. pertussis* and *C. violaceum* enzymes share an identity of 73% and a similarity of 86%. Details concerning the kinetic and structural data are presented.

MATERIALS AND METHODS

Cloning, Expression, and Purification. Genomic DNA samples from *B. pertussis* (ATCC BAA-589) and *C. violaceum* (ATCC 12472) were obtained from the American Type Culture Collection. The first dehydrogenase cloned for this study was that from *B. pertussis*. Using PrimeSTAR HS DNA polymerase (Takara BIO USA, Clontech Laboratories), the *wlbA* gene was PCR-amplified such that the forward primer 5′-AAAA*CATAT*-*G*AGCTCACTTCCCATCACCGATCGAAAAATCCG and the reverse primer 5′-AAAA*CTCGAG*TCAGTCCAGCGGCA-GGGGGATGCGCACGC added *Nde*I and *Xho*I cloning sites, respectively. The gene encoding the dehydrogenase from *C. violaceum* was PCR-amplified such that the forward primer 5′-AAAA*CATATG*ATAGTGATTCCTCCGATTACCGATCGC-AAGATCCG and the reverse primer 5′-AAA*CTCGAG*TTAG-TAATCCAGCGGCAGGCTGACGCGGCGGCC also added *Nde*I and *Xho*I cloning sites. Both purified PCR products were A-tailed and ligated into pGEM-T (Promega) vectors for screening and sequencing. The WlbA-pGEM-T vector constructs of the correct sequence were then appropriately digested and ligated into pET28JT vectors for protein production with a TEV protease cleavable N-terminal His_6 tag (*10*).

For production of the dehydrogenase from *B. pertussis*, the WlbA-pET28JT plasmid was used to transform *Escherichia coli* Rosetta(DE3) cells (Novagen). The culture was grown at 37 °C in LB media with shaking until the measured optical density at 600 nm was approximately 0.8, at which time the cell cultures were induced with 1.0 mM IPTG and then allowed to express protein at 21 °C for 18 h. WlbA was purified by standard procedures using NiNTA column chromatography at room temperature (with the lysis buffer containing 10% glycerol and all buffers containing 500 mM NaCl). Following purification, the protein was dialyzed against 10 mM Tris-HCl and 200 mM NaCl at pH 8.0 and then concentrated to 14 mg/mL on the basis of an extinction coefficient of 0.57 $(mg/mL)^{-1}$ cm^{-1}. Analysis by analytical ultracentrifugation showed the oligomerization state of the protein to be octameric (University of Wisconsin—Madison Biophysics Instrumentation Facility, supported by the University of Wisconsin—Madison and grants from the NSF (BIR-9512577) and the NIH (S10 RR13790)).

For production of the dehydrogenase from *C. violaceum*, the WlbA-pET28JT plasmid was used to transform *E. coli* Rosetta-(DE3) cells (Novagen). The culture was grown at 37 °C in LB media with shaking until the measured optical density at 600 nm was approximately 0.8, at which time the cultures were induced

Table 1: X-ray Data Collection Statistics

	MAD phasing data (*C. violaceum* WlbA)				
	peak	inflection	remote	*C. violaceum* WlbA	*B. pertussis* WlbA
resolution limits	50.0−1.90 (1.93−1.90)[b]	50−1.90 (1.93−1.90)[b]	50.0−1.90 (1.93−1.90)[b]	30.0−1.50 (1.53−1.50)[b]	30.0−2.13 (2.17−2.13)[b]
wavelength	0.97918	0.97953	0.97150	0.97921	0.97921
no. of independent reflections	32809 (1606)	32827 (1618)	32805 (1612)	63793 (2839)	297970 (12098)
completeness (%)	99.7 (100.0)	99.6 (100.0)	99.9 (100.0)	96.9 (87.1)	92.7 (75.5)
redundancy	14.1 (13.8)	14.1 (13.7)	14.3 (14.0)	9.0 (2.8)	3.8 (2.3)
avg I/avg $\sigma(I)$	51.5 (7.8)	52.0 (7.8)	47.8 (6.5)	47.4 (2.2)	27.8 (3.9)
R_{sym} (%)[a]	10.4 (32.2)	9.6 (29.9)	10.5 (39.3)	5.9 (28.3)	6.1 (16.1)

[a] $R_{sym} = (\sum|I - \bar{I}|/\sum I) \times 100$. [b] Statistics for the highest resolution bin.

with 1.0 mM IPTG and allowed to express protein at 21 °C for 18 h. WlbA was purified by standard procedures using NiNTA resin at room temperature (with the lysis buffer containing 10% glycerol). Following purification, TEV protease was added to the protein at a 50:1 protein:TEV ratio. The digestion was allowed to proceed overnight at room temperature, and subsequently the reaction mixture was dialyzed against 50 mM sodium phosphate (pH 8), 300 mM NaCl, and 20 mM imidazole. Cleaved protein was separated from the TEV protease and any undigested protein via NiNTA column chromatography. The cleaved protein was pooled and dialyzed against 10 mM Tris-HCl and 200 mM NaCl at pH 8.0 and then concentrated to 19 mg/mL on the basis of an extinction coefficient of 0.69 (mg/mL)$^{-1}$ cm^{-1}. Analysis by analytical ultracentrifugation determined the oligomerization state of this protein to be octameric as well.

Structural Analysis of WlbA. Crystallization conditions were initially surveyed with either the holoprotein or the protein incubated with 10 mM UDP-GlcNAcA. The hanging drop method of vapor diffusion was used along with a sparse matrix screen developed in the laboratory. The UDP-GlcNAcA ligand was prepared as previously described (*7*). For the *B. pertussis* enzyme, X-ray diffraction quality crystals were ultimately obtained via vapor diffusion by mixing in a 1:1 ratio the protein incubated with 10 mM UDP-GlcNAcA and a precipitant solution composed of 14−18% monomethyl ether poly(ethylene glycol) 5000, 200 mM NaCl, and 100 mM HEPPS (pH 8.5). The crystals belonged to the space group $P2_1$ with unit cell dimensions of a = 102.3 Å, b = 320.0 Å, c = 103.8 Å, and β = 119.1°. The asymmetric unit contained 16 monomers or 2 octamers. The crystals were stabilized for cryocooling by transferring them to a solution containing 25% monomethyl ether poly(ethylene glycol) 5000, 400 mM NaCl, 10 mM UDP-GlcNAcA, 18% 1,2-ethanediol, and 100 mM HEPPS (pH 8.5).

For the *C. violaceum* enzyme, X-ray diffraction quality crystals were grown via hanging drop by mixing in a 1:1 ratio the protein incubated with 10 mM UDP-GlcNAcA and a precipitant solution containing 15−19% monomethyl ether poly(ethylene glycol) 5000, 200 mM LiCl, and 100 mM HEPPS (pH 8.0). These crystals belonged to the space group $I422$ with unit cell dimensions of a = b = 106.7 Å, c = 143.4 Å, and one monomer per asymmetric unit. The crystals were stabilized for cryocooling by transferring them to a solution containing 24% monomethyl ether poly(ethylene glycol) 5000, 300 mM NaCl, 200 mM LiCl, 20% 1,2-ethanediol, and 100 mM HEPPS (pH 8.0).

Table 2: Model Refinement Statistics

	C. violaceum WlbA	*B. pertussis* WlbA
resolution limits (Å)	30.0−1.50	30.0−2.13
R-factor[a] (overall) (%)/no. of reflections	20.3/63793	18.7/297970
R-factor (working) (%)/no. reflections	20.1/60557	18.3/282933
R-factor (free) (%)/no. reflections	23.6/3236	26.9/15037
no. of protein atoms	2713[b]	42024[c]
no. of heteroatoms	354[d]	1961[e]
average B values		
protein atoms (Å^2)	25.2	41.1
ligands (Å^2)	27.8	35.1
solvent (Å^2)	33.7	41.1
weighted rms deviations from ideality		
bond lengths (Å)	0.013	0.005
bond angles (deg)	2.27	2.30
general planes (Å)	0.013	0.010

[a] R-factor = $(\sum|F_o - F_c|/\sum|F_o|) \times 100$, where F_o is the observed structure factor amplitude and F_c is the calculated structure factor amplitude. [b] These include multiple conformations for Arg 216, Asn 217, Ser 237, Val 240, and Arg 313. [c] These include multiple conformations for Arg 230 and His 280 in subunit B, Arg 228 in subunit D, Val 224 in subunit H, and Leu 344 in subunit L. [d] Heteroatoms include 1 NAD(H), 1 UDP-GlcNAcA, 1 sodium ion, 1 chloride ion, and 268 waters. [e] Heteroatoms include 16 NAD(H) molecules, 16 UDP-GlcNAcA ligands, and 617 waters.

X-ray data sets from flash-cooled crystals were collected at the Structural Biology Center Beamline 19-BM (Advanced Photon Source, Argonne National Laboratory, Argonne, IL). The data sets were processed and scaled with HKL3000 (*11*). X-ray data collection statistics are presented in Table 1.

An initial structure was determined using a selenomethionine-labeled version of the *C. violaceum* WlbA, which was prepared using standard methods and purified and crystallized in the same manner as that for the wild-type enzyme. Nine of the 13 possible selenium atoms were located by SOLVE (*12*), yielding an overall figure of merit of 0.64 to 1.9 Å resolution. A preliminary model was constructed with the software package COOT (*13*). The structure was then used as a search model for molecular replacement with PHASER (*14*) against the X-ray data set collected from a crystal of the wild-type protein. Refinement of the model with REFMAC (*15*) led to a final overall R-factor of 20.3% for all measured X-ray data from 30 to 1.5 Å resolution. Relevant refinement statistics are given in Table 2.

Table 3: Kinetic Parameters

	C. violaceum WlbA with UDP-GlcNAcA	*C. violaceum* WlbA with WlbC and UDP-GlcNAcA	*C. violaceum* WlbA with UDP-GlcA	*B. pertussis* WlbA with UDP-GlcNAcA	*B. pertussis* WlbA with WlbC and UDP-GlcNAcA	*B. pertussis* WlbA with UDP-GlcA
WlbA concn (μM)	24.5	6.1	23.0	14.4	4.9	14.4
K_m(UDP-sugar) (mM)	1.10 ± 0.08	0.0056 ± 0.0008	0.20 ± 0.02	2.36 ± 0.35	0.015 ± 0.002	2.05 ± 0.21
K_m(NAD^+) (mM)	0.47 ± 0.07	0.089 ± 0.009	0.45 ± 0.06	0.97 ± 0.04	0.055 ± 0.007	0.95 ± 0.05
V_{max} (μM/min)	0.46 ± 0.02	0.28 ± 0.01	0.12 ± 0.01	4.09 ± 0.07	1.13 ± 0.04	1.80 ± 0.14
k_{cat} (s^{-1})	0.00031 ± 0.00001	0.00076 ± 0.00003	0.00015 ± 0.00001	0.0047 ± 0.0001	0.0039 ± 0.0002	0.0021 ± 0.0001
k_{cat}/K_m (M^{-1} s^{-1}), UDP-linked sugar	0.28	135	0.75	2.0	260	1.0

The structure of the *B. pertussis* enzyme was determined via molecular replacement with PHASER using as a search model the monomer of the *C. violaceum* enzyme in which all ligands and solvent molecules had been removed. Iterative rounds of refinement with REFMAC, 16-fold molecular averaging with the software package DM (*16*), and model building with COOT led to a final overall *R*-factor of 18.7% for all measured X-ray data from 30 to 2.13 Å resolution. Relevant refinement statistics are presented in Table 2.

Measurement of Enzymatic Activity. Enzymatic activities of both the *B. pertussis* and *C. violaceum* dehydrogenases were monitored spectrophotometrically by following the increase in absorbance at 340 nm due to the conversion of NAD^+ to NADH. Reactions were monitored continuously with a Beckman DU 640B spectrophotometer, and enzyme activities were calculated from the initial rates. For the *C. violaceum* enzyme, assay mixtures were 0.75 mL in volume and contained 0.5 mg/mL enzyme, 100 mM NaCl, and 50 mM HEPPS (pH 8.5). Initial velocity patterns were evaluated by measuring the initial rates at four concentrations of each substrate: 7.0, 1.06, 0.56, and 0.35 mM UDP-GlcNAcA and 7.5, 4.0, 0.56, and 0.27 mM NAD^+. The reactions were run at 25 °C and initiated by the addition of the enzyme. Equation 1 was used to fit the data with the program SigmaPlot8. Kinetic parameters are listed in Table 3.

$$v = VAB/(K_aB + K_bA + K_{ia}K_b + AB) \quad (1)$$

The *B. pertussis* enzyme was analyzed in a similar manner, using NAD^+ concentrations of 15.0, 2.5, 1.0, and 0.4 mM and UDP-GlcNAcA concentrations of 23.6, 6.9, 2.0, and 0.75 mM. Kinetic parameters are presented in Table 3.

UDP-glucose, UDP-galactose, UDP-GlcNAc, and UDP-GlcA were screened as possible substrates for WlbA. Of the four, only UDP-GlcA was converted into a 3-keto sugar. Kinetic parameters were determined for both enzymes using UDP-GlcA as a substrate. The parameters for NAD^+ were also measured again to ensure that UDP-GlcA did not perturb the binding of the dinucleotide. These parameters were determined via saturation kinetics and the data fitted to eq 2.

$$v = VA/(K_a + A) \quad (2)$$

The kinetic parameters are listed in Table 3.

We were also interested in determining if there was an enhancement in UDP-GlcNAcA binding or turnover in the presence of the next enzyme in the pathway, the aminotransferase WlbC, which converts the 3-keto sugar generated by WlbA into a 3-amino sugar (Scheme 1). Similar assay conditions were used with an excess of glutamate (30 mM) and varying the amount of WlbC until it was determined at what point it was not a limiting reagent in the assay. This occurred when the amount of WlbC was in at least a 2× molar excess over the amount of WlbA. Kinetic parameters were then determined by measuring the formation of NADH, starting with the original assay conditions, the addition of 30 mM glutamate, and a 2.5 molar excess of WlbC over WlbA. The NAD^+ and UDP-GlcNAcA concentrations were varied as needed. Binding constants were determined using saturation kinetics and fitted to eq 2. These kinetic parameters are also presented in Table 3.

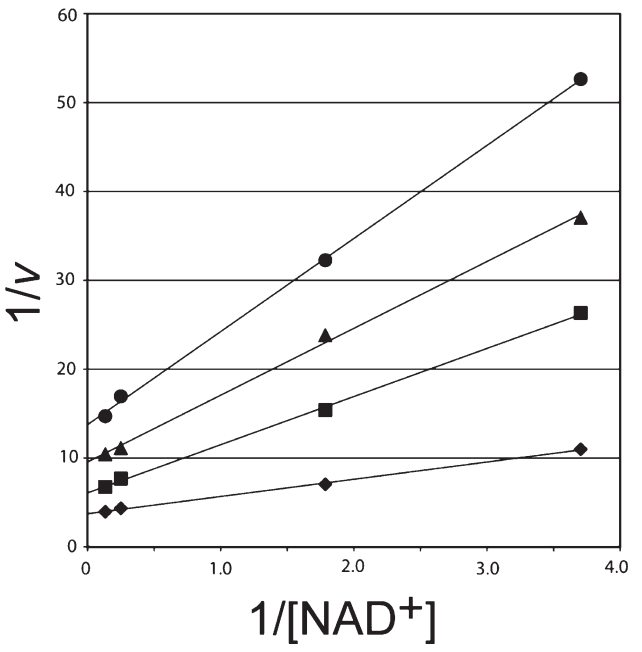

FIGURE 2: Double reciprocal plots for the initial rates of formation of NADH using the *C. violaceum* enzyme. The concentration of NAD^+ was varied at 7.5, 4.0, 0.56, and 0.27 mM at several fixed concentrations of UDP-GlcNAcA: 7.0 mM (diamond), 1.06 mM (square), 0.56 mM (triangle), and 0.35 mM (circle). Initial velocities (v) are expressed in micromolar per minute of NADH formation.

RESULTS AND DISCUSSION

Functional Analysis of WlbA from B. pertussis and C. violaceum. In previous investigations, the *P. aeruginosa* WlbA was shown to employ a ping-pong catalytic mechanism and to use an NAD^+ recycling pathway that couples WlbA and WlbC together (*6*, *7*). As indicated in Scheme 1, WlbC is an aminotransferase that catalyzes an amination step in the biosynthesis of UDP-ManNAc3NAcA. Assuming that the *B. pertussis* and *C. violaceum* dehydrogenases would function in a similar manner to that of the *P. aeruginosa* enzyme, we initially attempted to monitor UDP-3-keto-GlcNAcA formation via an HPLC assay as previously described (*7*). It was expected that an

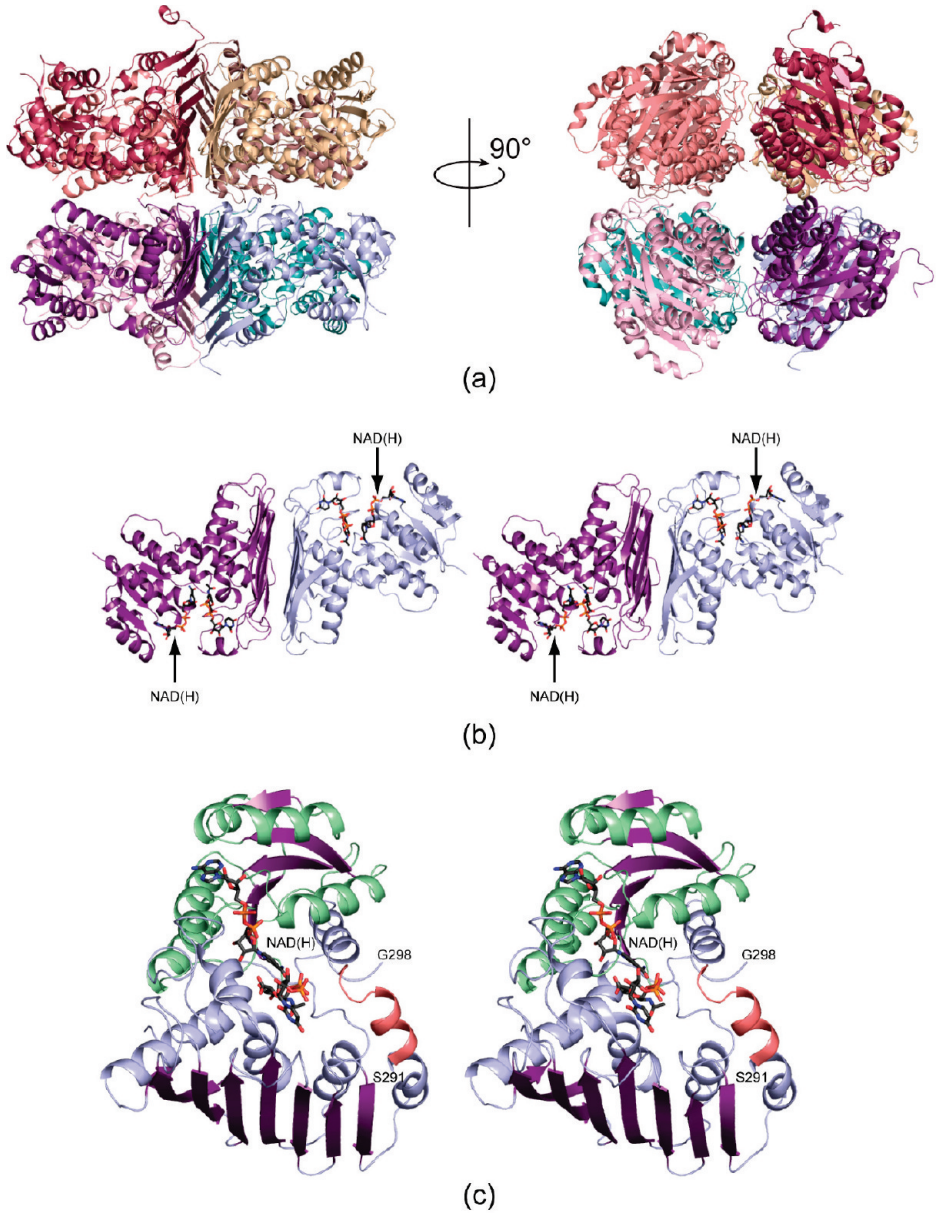

FIGURE 3: The structures of WlbA from *B. pertussis* and *C. violaceum*. Both enzymes adopt octameric quaternary structures with 422 symmetry. Shown in (a) are two ribbon representations for the *B. pertussis* enzyme rotated 90° apart. The right-hand panel shows the molecule viewed down the 4-fold rotational axis. The octamers can be thought of as tetramers of dimers. One such dimer is displayed in stereo in (b). The bound NAD(H) and UDP-GlcNAcA molecules are depicted in stick representations. A close-up view of an individual subunit from the *C. violaceum* WlbA is presented in (c). The α-helices and β-strands for the N-terminal domain are highlighted in light green and purple, respectively, whereas those in the C-terminal domain are color-coded in light blue and purple. The α-helix displayed in salmon indicates the conformation of the region in the *B. pertussis* enzyme that is disordered in the *C. violaceum* protein.

observable reaction yielding UDP-3-keto-GlcNAcA would result by mixing WlbA, UDP-GlcNAcA, WlbC, and glutamate. To our surprise, no reaction occurred. Similarly, no catalysis occurred if a reaction mixture of WlbA and UDP-GlcNAcA alone was spiked with α-ketoglutarate in the absence of the aminotransferase enzyme. In contrast, this same type of reaction mixture yielded UDP-3-keto-GlcNAcA in assays with the *P. aeruginosa* enzyme (*6*, *7*). It was finally determined that the reaction required the addition of an equimolar ratio of NAD^+ to UDP-GlcNAcA for both the *B. pertussis* and *C. violaceum* enzymes to catalyze the formation of UDP-3-keto-GlcNAcA.

Kinetic parameters were subsequently determined for both the *B. pertussis* and *C. violaceum* enzymes by monitoring spectrophotometrically the conversion of NAD^+ to NADH. For both enzymes, double reciprocal plots clearly showed a series of intersecting lines indicative of a sequential mechanism (Figure 2). The activities of the *B. pertussis* and *C. violaceum* enzymes were also tested against UDP-glucose, UDP-galactose, UDP-GlcNAc, and UDP-GlcA. Neither enzyme could turnover UDP-glucose, UDP-galactose, or UDP-GlcNAc, but both were able to function on UDP-GlcA. Relevant kinetic parameters for the enzymes using UDP-GlcA as a substrate are given in Table 3. As discussed below, the carboxylate group attached to the C-5′ carbon of the hexose in the natural substrate, UDP-GlcNAcA, is held firmly in place in the WlbA active site by the side chains of Arg 165 and Tyr 169. Most likely, the absence of this carboxylate group, as in the case of UDP-glucose, UDP-galactose, or UDP-GlcNAc, results in either no binding or nonproductive binding to WlbA. The fact that WlbA can turn over UDP-GlcA also suggests that an *N*-acetyl group at the C-2′ position of the hexose,

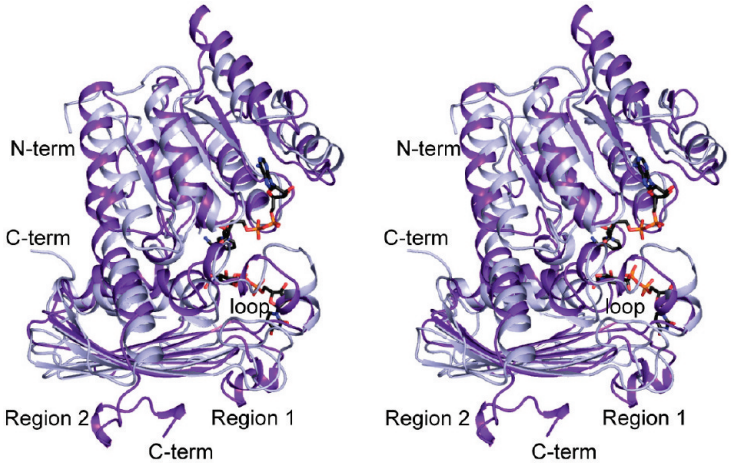

FIGURE 4: Superposition of the ribbon representations for the *P. aeruginosa* and *C. violaceum* enzymes. The *P. aeruginosa* and *C. violaceum* WlbAs are highlighted in purple and light blue, respectively. X-ray coordinates for the *P. aeruginosa* enzyme were determined in this laboratory and deposited in the Protein Data Bank (accession number 3OA0).

as in UDP-GlcNAcA, is not important for proper substrate positioning. Indeed, as described below, the *N*-acetyl group of UDP-GlcNAcA, when bound in the enzyme active site, is simply surrounded by water molecules.

The catalytic efficiencies of the enzymes from *C. violaceum* and *B. pertussis* were determined to be 0.28 and 2.0 M^{-1} s^{-1}, respectively (Table 3). These values are significantly reduced from those measured for the *T. thermophilus* and *P. aeruginosa* enzymes (5.6×10^5 and 2.2×10^7 M^{-1} s^{-1}, respectively) (*7*). Given the low catalytic efficiencies for the *C. violaceum* and *B. pertussis* enzymes, the question was raised as to whether the genes encoding them were correctly annotated. Recent investigations by Westman et al., using complementation analyses of *wlbA* knockout mutants, document that WlbA from *B. pertussis* functions in UDP-ManNAc3NAcA biosynthesis and that it catalyzes the reported oxidation reaction (*4*). Regardless of the low catalytic efficiencies measured *in vitro*, these enzymes clearly support function *in vivo*.

We were curious as to whether the addition of WlbC, the next enzyme in the biosynthetic pathway (Scheme 1), would have any effect on the kinetic parameters of the *B. pertussis* and *C. violaceum* enzymes. The catalytic efficiencies for both enzymes improved to 135 and 260 M^{-1} s^{-1}, respectively (Table 3). With respect to the *C. violaceum* enzyme, the K_m for the UDP-linked sugar dropped from 1.10 to 0.0056 mM, whereas the K_m for the NAD^+ cofactor dropped from 0.47 to 0.089 mM. Likewise, the same trend occurred with the *B. pertussis* WlbA. Specifically the K_m for the UDP-linked sugar was reduced from 2.36 to 0.015 mM, whereas the K_m for the NAD^+ cofactor was reduced from 0.97 to 0.055 mM. These data are highly suggestive of some type of protein−protein interaction occurring between WlbA and WlbC *in vivo*, and, indeed, this coupling phenomenon between the dehydrogenase and the aminotransferase has been previously reported for the *P. aeruginosa* enzyme (*5*, *6*). Interestingly, if the reactions were conducted using UDP-GlcA as the substrate rather than UDP-GlcNAcA, the same enhancement of catalytic efficiency was not observed, and the kinetic parameters were essentially unchanged as listed in Table 3.

Structure of WlbA. Crystals of the *B. pertussis* WlbA belonged to the space group $P2_1$ with two octamers in the asymmetric unit. They diffracted to a nominal resolution of 2.13 Å. Overall, the polypeptide chains corresponding to the 16 subunits in the asymmetric unit were reasonably well ordered with only a few breaks in the electron densities. The Ramachandran statistics, as calculated according to PROCHECK (*17*), are good with 87.5%, 12.2%, and 0.3% of the ϕ,ψ torsional angles lying within the core, allowed, and generously allowed regions.

Shown in Figure 3a is a ribbon representation of one of the octamers. It has overall dimensions of approximately $110 \times 100 \times 115$ Å and displays 422 symmetry. It can be aptly described as a tetramer of dimers. A stereoview of one of the dimers is shown in Figure 3b. The quaternary structure of the *B. pertussis* WlbA is completely different from that observed for WlbA from *P. aeruginosa* (Figure 1) even though the individual subunits have similar folds with one major exception as discussed below. In the *B. pertussis* enzyme, the active sites within the dimeric unit are positioned at greater than 40 Å apart and are contained within the individual subunits. This is in sharp contrast to the *P. aeruginosa* enzyme whereby the active sites are formed between subunits of the tetramer and lie closely to one another. The surface area buried per subunit upon formation of the *B. pertussis* octamer is approximately 3400 $Å^2$. The C-terminal tails of each subunit project towards the interface of the octamer, and this is in keeping with the fact that placing a purification tag at the C-terminus of the *B. pertussis* WlbA always resulted in the expression of insoluble protein in *E. coli*.

The *C. violaceum* WlbA crystallized in the space group *I*422 with one subunit per asymmetric unit. Its quaternary structure is still octameric, however, as indicated by both crystalline packing considerations and analytical ultracentrifugation experiments. The overall folds of the *C. violaceum* and *B. pertussis* enzymes are similar such that their α-carbons superimpose with a root-mean-square deviation of 1.6 Å. Given their similarities in both amino acid sequences and three-dimensional structures, and the fact that the crystals of the *C. violaceum* WlbA diffracted to a higher resolution of 1.5 Å, the following discussion refers only to the *C. violaceum* enzyme unless otherwise indicated.

The model for the *C. violaceum* WlbA is excellent with 91.7% and 8.3% of the ϕ,ψ angles lying within the core and allowed regions of the Ramachandran plot, respectively. A close-up view of the single subunit in the asymmetric unit is presented in Figure 3c. Both Met 1 and the C-terminal Tyr 351 are visible in the electron density map. Three proline residues, at positions 105, 246, and 348, adopt *cis* conformations, and these *cis* prolines are

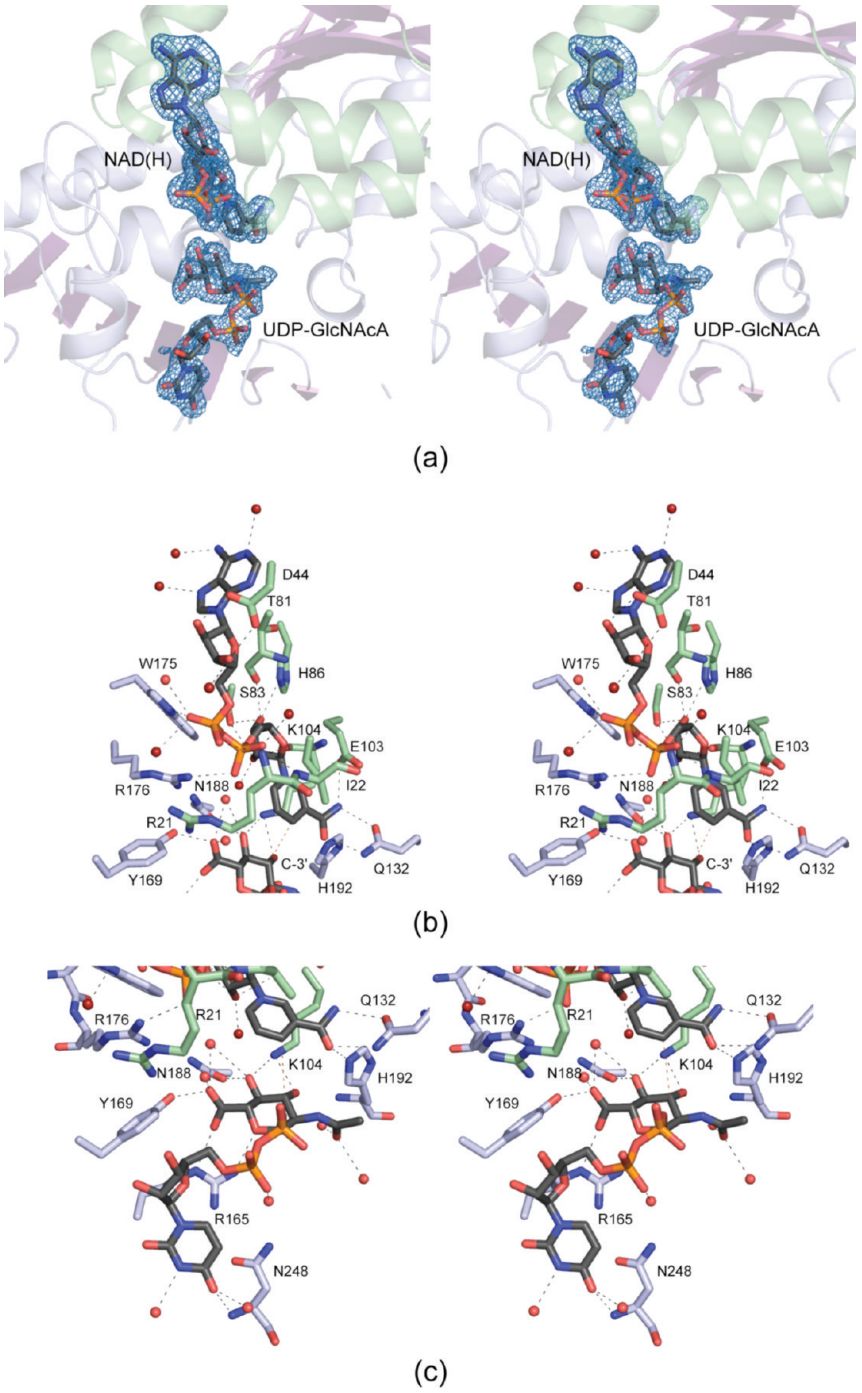

FIGURE 5: The active site for the *C. violaceum* WlbA. Electron densities corresponding to the bound ligands are shown in (a). The electron density map, contoured at 2.5σ, was calculated with coefficients of the form ($F_o - F_c$), where F_o was the native structure factor amplitude and F_c was the calculated structure factor amplitude. A close-up view of the active site near NAD(H) is depicted in (b). The dashed lines indicate possible hydrogen bonds. Water molecules are represented as red spheres. The residues colored in green and blue belong to the N- and C-terminal domains, respectively. The red dashed line between the hexose C-3′ carbon and the nicotinamide C-4 carbon illustrates how the sugar moiety is ideally oriented in the active site for direct hydride transfer. A close-up view of the active site near the UDP-GlcNAcA ligand is presented in (c).

conserved in the *B. pertussis* enzyme. Pro 105 is positioned near the nicotinamide ribose of the NAD(H) ligand, Pro 246 resides in a loop near the uracil group of the nucleotide-linked sugar, and Pro 348 sits close to the C-terminus, far removed from the active site cleft. Note that because the oxidation state of the dinucleotide is unknown, it will be referred to as NAD(H).

Overall, the WlbA subunit can be described in terms of two domains: an N-terminal Rossmann fold defined by Met 1 to Lys 131 and a C-terminal region delineated by Gln 132 to Tyr 351. The N-terminal region, which provides the binding scaffold for the dinucleotide cofactor, is dominated by a decidedly twisted six-stranded parallel β-sheet flanked on each side by three α-helices. The C-terminal domain, which harbors the binding site for UDP-GlcNAcA, consists of an eight-stranded mixed β-sheet surrounded by four α-helices on one side. The other side of the β-sheet provides the subunit−subunit interface of the "dimer" in the octamer (Figure 3b). As can be seen in Figure 3c, the C-terminal domain provides one of the α-helices flanking the β-sheet in

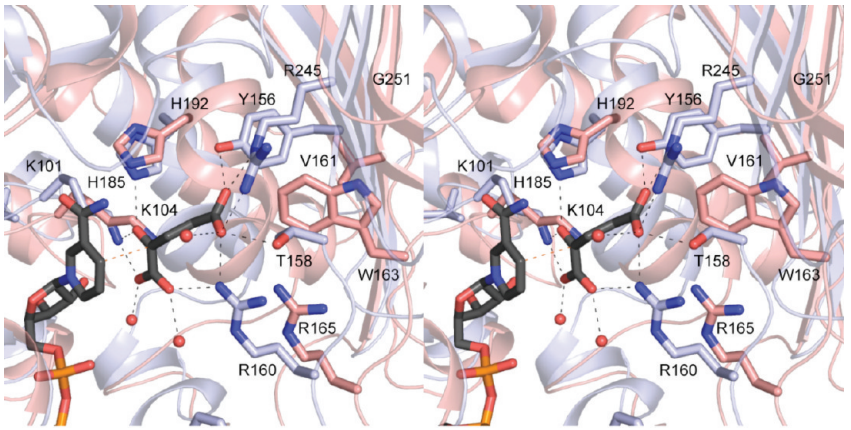

FIGURE 6: Binding site for α-ketoglutarate in the *P. aeruginosa* WlbA. The ribbon representation displayed in blue corresponds to the *P. aeruginosa* WlbA, and those residues forming hydrogen bonds with α-ketoglutarate are displayed in light blue bonds. The structurally equivalent region in the *C. violaceum* enzyme is shown in salmon.

the N-terminal Rossmann fold. There is only one break in the *C. violaceum* model between Ser 291 and Gly 298. In the *B. pertussis* enzyme, the structurally equivalent region adopts two turns of an α-helix and lies near the opening to the active site (Figure 3c).

The subunits for the WlbA enzymes from *C. violaceum* and *P. aeruginosa* superimpose with a root-mean-square deviation of 1.7 Å for 257 structurally equivalent α-carbons. Why are their quaternary structures so different? A superposition of their polypeptide chains, as presented in Figure 4, provides the answer. The N-terminus of the *C. violaceum* enzyme is longer by ten residues. This extended N-terminal tail projects towards the adenine ring of the NAD(H) in a 4-fold-related monomer of the octamer. There is also an eight-residue insertion in the *C. violaceum* WlbA between Thr 213 and Asp 222, which projects towards another monomer of the octamer (labeled "loop" in Figure 4). The biggest differences in the two proteins occur at Tyr 245 (*C. violaceum* WlbA numbering) and at their C-termini. These areas are labeled regions 1 and 2, respectively, in Figure 4. In the *P. aeruginosa* WlbA, there is a ten-residue insertion that adopts a helical conformation and abuts the large mixed β-sheet of the C-terminal domain. Likewise, the C-terminal residues in the *P. aeruginosa* WlbA lie against this β-sheet, whereas in the *C. violaceum* WlbA, they curl away to form another β-strand (Figure 4). Taken together, these two regions in the *P. aeruginosa* WlbA preclude it from forming a subunit−subunit interface that involves the large mixed β-sheet of the C-terminal domain.

Electron densities corresponding to the bound NAD(H) and UDP-GlcNAcA ligands are displayed in Figure 5a. The nucleotide-linked sugar adopts an extended conformation which is in stark contrast to that observed for the *P. aeruginosa* WlbA where the C-5 carbon of the uracil ring and the C-6′ carbon of the hexose reside within 3.7 Å of each other. The carboxamide group of the NAD(H) is twisted out of the plane of the ring.

A close-up view of the NAD(H) binding pocket is presented in Figure 5b. Both riboses of the dinucleotide adopt the C2′-endo pucker. The adenine ring projects outward towards the solvent and is surrounded by three water molecules. The adenine ribose is hydrogen bonded to the carboxylate of Asp 44 and one water molecule. Both Trp 175 and Arg 176 provide hydrogen-bonding interactions with the phosphoryl groups of the cofactor. Three waters and the backbone amides of Arg 21 and Ile 22 provide additional interactions with the phosphoryl groups. The nicotinamide/ribose portion of the cofactor is positioned into the active site via one water molecule, the side chains of Ser 83, His 86, Glu 103, and Gln 132, and the backbone carbonyls of Thr 81 and Lys 104.

Shown in Figure 5c is a close-up view of the UDP-GlcNAcA binding site. As in the case of the adenine ring in NAD(H), the uracil group is located towards the solvent. It is surrounded by two water molecules and lies within hydrogen-bonding distance of the backbone amide group of Asn 248. Only one well-ordered water molecule is situated within 3.2 Å of the phosphoryl groups of the UDP-linked sugar substrate. The *N*-acetyl group at position C-2′ is surrounded by two water molecules. The C-3′ hydroxyl, which is ultimately oxidized to a keto group, lies at 3.0 Å from the ε-nitrogen of Lys 104. Most likely, Lys 104 serves as the catalytic base to abstract the proton from the C-3′ hydroxyl group. The side chain of Lys 104 also lies within 3.0 Å of the C-4′ hydroxyl, which is further surrounded by the side chain of Asn 188 and a water molecule. Note that Lys 104 is conserved in the *P. aeruginosa* and *T. thermophilus* enzymes as well. Finally, the C-5′ carboxylate group of the hexose is anchored to the protein through interactions with the side chains of Arg 165 and Tyr 169 and two water molecules. The hexose C-3′ carbon atom, which loses a hydride to NAD^+ during catalysis, faces the *re* face of the nicotinamide ring of the cofactor and sits at 4.0 Å from the cofactor C-4 carbon. The mode of NAD(H) and UDP-GlcNAcA binding to the *C. violaceum* WlbA is nearly identical to that observed for the *B. pertussis* enzyme except that, in the latter protein, Arg 20 projects into the active site where it forms electrostatic interactions with the phosphoryl groups of UDP-GlcNAcA.

As noted above, the *B. pertussis* and *C. violaceum* WlbA enzymes do not undergo the cofactor recycling mechanism observed for the *P. aeruginosa* enzyme. A close-up view of the binding pocket for α-ketoglutarate, as observed in the *P. aeruginosa* WlbA, is shown in Figure 6. Key residues involved in binding α-ketoglutarate include Lys 101, Tyr 156, Thr 158, Arg 160, His 185, and Arg 245. Three of these residues, Lys 101, His 185, and Arg 160, are retained as Lys 104, His 192, and Arg 165 in the *C. violaceum* enzyme (Figure 6). Tyr 156, Thr 158, and Arg 245, which form electrostatic interactions with the side chain carboxylate of α-ketoglutarate in the *P. aeruginosa* WlbA active site, are replaced with Val 161, Trp 163, and Gly 251, respectively, in the *C. violaceum* active site. These changes in amino acid residues preclude the binding of α-ketoglutarate into the active site of the *C. violaceum* WlbA.

In summary, the results presented here demonstrate that there are two families of WlbA enzymes involved in the biosynthesis of

UDP-ManNAc3NAcA, which we will refer to as class A and class B. With respect to primary structure, family members can be distinguished on the basis of their amino acid sequences. Within the class A or class B families, members typically demonstrate greater than 45% amino acid sequence identity. Between classes, however, the amino acid sequence identity is less than 15%. The class A members, defined by the *P. aeruginosa* WlbA, adopt unusual tetrameric structures with their active sites positioned between subunits and their nucleotide-linked sugars adopting highly curved conformations. Additionally, these enzymes employ α-ketoglutarate in their NAD^+ recycling systems, at least *in vitro*, and they display ping-pong reaction mechanisms. Contrastingly, members of the class B family, defined by the *B. pertussis* WlbA, function as octamers, display sequential reaction kinetics, and cannot accommodate α-ketoglutarate in their active sites. These differences in the structures and mechanisms of the two WlbA families have important ramifications for the potential design of new therapeutics in the treatment of *P. aeruginosa* and *B. pertussis* infections.

ACKNOWLEDGMENT

A portion of the research described in this paper was performed at Argonne National Laboratory, Structural Biology Center at the Advanced Photon Source (United States Department of Energy, Office of Biological and Environmental Research under Contract DE-AC02-06CH11357). We gratefully acknowledge Dr. Norma E. C. Duke for assistance during the X-ray data collection at Argonne and Professor W. W. Cleland for helpful discussions.

REFERENCES

1. Knirel, Y. A., and Kochetkov, N. K. (1994) Structure of lipopolysaccharides from Gram-negative bacteria. III. Structure of *O*-specific polysaccharides. *Biokhimiya 59*, 1784–1851.
2. Harvill, E. T., Preston, A., Cotter, P. A., Allen, A. G., Maskell, D. J., and Miller, J. F. (2000) Multiple roles for *Bordetella* lipopolysaccharide molecules during respiratory tract infection. *Infect. Immun. 68*, 6720–6728.
3. Schaeffer, L. M., McCormack, F. X., Wu, H., and Weiss, A. A. (2004) *Bordetella pertussis* lipopolysaccharide resists the bactericidal effects of pulmonary surfactant protein A. *J. Immunol. 173*, 1959–1965.
4. Westman, E. L., Preston, A., Field, R. A., and Lam, J. S. (2008) Biosynthesis of a rare di-*N*-acetylated sugar in the lipopolysaccharides of both *Pseudomonas aeruginosa* and *Bordetella pertussis* occurs via an identical scheme despite different gene clusters. *J. Bacteriol. 190*, 6060–6069.
5. Westman, E. L., McNally, D. J., Charchoglyan, A., Brewer, D., Field, R. A., and Lam, J. S. (2009) Characterization of WbpB, WbpE, and WbpD and reconstitution of a pathway for the biosynthesis of UDP-2,3-diacetamido-2,3-dideoxy-D-mannuronic acid in *Pseudomonas aeruginosa*. *J. Biol. Chem. 284*, 11854–11862.
6. Larkin, A., and Imperiali, B. (2009) Biosynthesis of UDP-GlcNAc-(3NAc)A by WbpB, WbpE, and WbpD: enzymes in the Wbp pathway responsible for *O*-antigen assembly in *Pseudomonas aeruginosa* PAO1. *Biochemistry 48*, 5446–5455.
7. Thoden, J. B., and Holden, H. M. (2010) Structural and functional studies of WlbA: a dehydrogenase involved in the biosynthesis of 2,3-diacetamido-2,3-dideoxy-D-mannuronic acid. *Biochemistry 49*, 7939–7948.
8. Kingston, R. L., Scopes, R. K., and Baker, E. N. (1996) The structure of glucose-fructose oxidoreductase from *Zymomonas mobilis*: an osmoprotective periplasmic enzyme containing non-dissociable NADP. *Structure 4*, 1413–1428.
9. Lichstein, H. C., and Van De Sand, V. F. (1946) The antibiotic activity of violacein, prodigiosin, and phthiocol. *J. Bacteriol. 52*, 145–146.
10. Thoden, J. B., Timson, D. J., Reece, R. J., and Holden, H. M. (2005) Molecular structure of human galactokinase: implications for Type II galactosemia. *J. Biol. Chem. 280*, 9662–9670.
11. Minor, W., Cymborowski, M., Otwinowski, Z., and Chruszcz, M. (2006) HKL-3000: the integration of data reduction and structure solution-from diffraction images to an initial model in minutes. *Acta Crystallogr., Sect. D: Biol. Crystallogr. 62*, 859–866.
12. Terwilliger, T. C., and Berendzen, J. (1999) Automated MAD and MIR structure solution. *Acta Crystallogr., Sect. D: Biol. Crystallogr. 55* (Part 4), 849–861.
13. Emsley, P., and Cowtan, K. (2004) Coot: model-building tools for molecular graphics. *Acta Crystallogr., Sect. D: Biol. Crystallogr. 60*, 2126–2132.
14. McCoy, A. J., Grosse-Kunstleve, R. W., Adams, P. D., Winn, M. D., Storoni, L. C., and Read, R. J. (2007) Phaser crystallographic software. *J. Appl. Crystallogr. 40*, 658–674.
15. Murshudov, G. N., Vagin, A. A., and Dodson, E. J. (1997) Refinement of macromolecular structures by the maximum-likelihood method. *Acta Crystallogr., Sect. D: Biol. Crystallogr. 53*, 240–255.
16. Cowtan, K. (1994) "DM": an automated procedure for phase improvement by density modification. *Joint CCP4 ESF-EACBM Newsl. Protein Crystallogr. 31*, 34–38.
17. Laskowski, R. A., MacArthur, M. W., Moss, D. S., and Thornton, J. M. (1993) PROCHECK: a program to check the stereochemical quality of protein structures. *J. Appl. Crystallogr. 26*, 283–291.
18. DeLano, W. L. (2002) The PyMOL Molecular Graphics System, DeLano Scientific, San Carlos, CA.